Inorganic Chemistry

ARTICLE

pubs.acs.org/IC

Bond Shortening (1.4 Å) in the Singlet and Triplet Excited States of $[Ir_2(dimen)_4]^{2+}$ in Solution Determined by Time-Resolved X-ray Scattering

Kristoffer Haldrup,[*,†] Tobias Harlang,[‡] Morten Christensen,[‡,§] Asmus Dohn,[‡] Tim Brandt van Driel,[‡] Kasper Skov Kjær,[‡] Niels Harrit,[‡,§] Johan Vibenholt,[§] Laurent Guerin,[∥] Michael Wulff,[∥] and Martin Meedom Nielsen[†]

[†]Centre for Molecular Movies, Technical University of Denmark, Risø National Laboratory, Materials Department, Roskilde, Denmark
[‡]Centre for Molecular Movies and [§]Chemistry Department, University of Copenhagen, Nano Science Centre, Copenhagen, Denmark
[∥]European Synchrotron Radiation Facility, Grenoble Cedex 38043, France

Supporting Information

ABSTRACT: Ground- and excited-state structures of the bimetallic, ligand-bridged compound $Ir_2(dimen)_4^{2+}$ are investigated in acetonitrile by means of time-resolved X-ray scattering. Following excitation by 2 ps laser pulses at 390 nm, analysis of difference scattering patterns obtained at eight different time delays from 250 ps to 300 ns yields a triplet excited-state distance between the two Ir atoms of 2.90(2) Å and a triplet excited-state lifetime of 410(70) ns. A model incorporating the presence of two ground-state structures differing in Ir−Ir separation is demonstrated to fit the obtained data very well, in agreement with previous spectroscopic investigations. Two ground-state isomers with Ir−Ir separations of 3.60(9) and 4.3(1) Å are found to contribute equally to the difference scattering signal at short time delays. Further studies demonstrate the feasibility of increasing the effective time resolution from the ∼100 ps probe width down to the 10 ps regime by positioning the laser pump pulse at selected points in the X-ray probe pulse. This approach is used to investigate the structures of both the singlet and the triplet excited states of $Ir_2(dimen)_4^{2+}$.

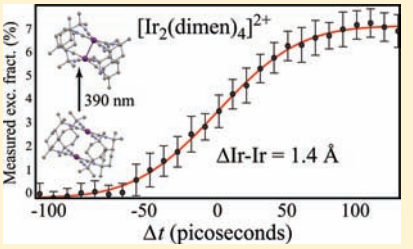

INTRODUCTION

Since their first synthesis in 1976,[1] the binuclear ligand-bridged "windmill" complexes of the general form $M_2(bridge)_4^{2+}$ (M = Ir, Rh) (Figure 1A) have received significant attention due to their redox activity and ability to facilitate photoinduced hydrogen evolution.[2] The high reactivity of the triplet excited state of these and related compounds prompted much subsequent research on determining the structure−function relationship of the excited state, leading to the highly detailed spectroscopic characterization presented for $Rh_2(dimen)_4^{2+}$ (dimen =1,8-diisocyano-*p*-menthane) by Miskowski et al. in 1994.[3] Through these and related studies (cf. the review by P. Harvey[4] and the later theoretical investigation of $Rh_2(1,3\text{-diisocyanopropane})_4^{2+}$[5]), it was concluded that the excited state of $M_2(bridge)_4^{2+}$ complexes exhibits pronounced conformational changes compared to the ground state, including a significant shortening of the metal−metal distance. This conclusion was confirmed by low-temperature time-resolved crystallographic measurements in 2004 when Coppens et al. succeeded in directly measuring a very large (0.86 Å) shortening of the Rh−Rh distance from 4.50 to 3.64 Å in PF_6 crystals of $Rh_2(dimen)_4^{2+}$[6] following electronic excitation. This shortening is only slightly less than the value derived from spectroscopic data by Miskowski et al.[3] However, no direct determination of the excited-state structure has been undertaken under the less constraining conditions in liquid solution, and no information regarding the excited-state structure has been reported for the iridium analogue $Ir_2(dimen)_4^{2+}$. The present study addresses both of these issues to shed light on solution-state structures in

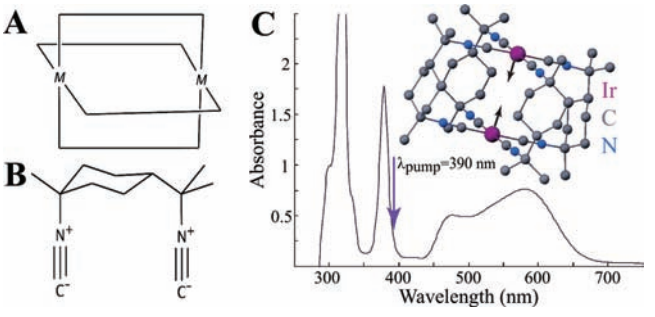

Figure 1. (A) Schematic depiction of the $M_2(bridge)_4^{2+}$ complexes. In the present work, the metal centers are Ir atoms and bridging ligands are the asymmetric dimen units for which the molecular structure is shown in B. (C) Absorption spectrum of $Ir_2(dimen)_4^{2+}$ in acetonitrile. Excitation is expected to be associated with a contraction of the two Ir atoms along their connecting vector, as depicted in the insert. For the experiments reported here, the excitation wavelength was 390 nm.

Received: April 5, 2011
Published: August 08, 2011

general and in particular on the excited-state structures of this class of bimetallic transition-metal compounds.

The structure of $Ir_2(dimen)_4^{2+}$ in its ground state is shown schematically in Figure 1. The two metal atoms are connected by four dimen units, giving rise to a ligand framework with a square-planar isocyanide configuration in the end groups (Figure 1A and 1B). In the crystalline state, the distance between the two Ir atoms is known to be strongly dependent on the crystal packing forces, with the distance varying from 3.60 Å in the $B(C_6H_5)_4$ salt to 4.41 Å in the PF_6 salt. Shortening of the Ir−Ir distance is associated with a ligand twist of 16° in the $B(C_6H_5)_4$ salt.[7] The significant flexibility of the ligand framework and corresponding variation in M−M distances is further established in crystallographic studies utilizing end-on adducts and Ag^+ encapsulation for which the Ir−Ir distances were reported as 2.986[8] and 5.28 Å,[9] respectively. Again, the shortest distance is associated with a significant ligand twist of 39°. Such large variation in the metal distance is in good agreement with the spectroscopy-based calculations,[3] where the ground-state distance between the metal atoms in the $M_2(dimen)_4^{2+}$ compounds was found to be determined by a very shallow potential governed primarily by the dimen ligands.

Figure 1C shows the absorption spectrum of $Ir_2(dimen)_4^{2+}$ in acetonitrile solution at room temperature. It differs from the spectrum obtained in the crystalline state[7] in displaying two overlapping transitions in the region of the metal-centered $d\sigma^* \rightarrow p\sigma$ transition at 450−650 nm. This observation was made by Exstrom et al. and interpreted as being due to different metal−metal separations among the $Ir_2(dimen)_4^{2+}$ molecules.[7] Specifically, the absorption spectrum in solution was interpreted as arising from two coexisting populations of $Ir_2(dimen)_4^{2+}$ with Ir−Ir distances close to 3.6 and 4.4 Å, respectively. The single-maximum emission spectrum (not shown) was interpreted as arising from only one excited-state population in terms of Ir−Ir distance. This was very recently supported by ultrafast transient absorption spectroscopy,[10] but further information on the photophysical properties of $Ir_2(dimen)_4^{2+}$ is scarce, as the emission quantum yields are low, and no information regarding the lifetime of the excited state appears to have been published.

For the experiments reported here, excitation of $Ir_2(dimen)_4^{2+}$ was at 390 nm, which is on the long-wavelength side of the ~375 nm peak associated with the $d_{xz,yz} \rightarrow p\sigma$ transition. Assuming direct analogy with the $Rh_2(TMB)_4^{2+}$ complex (TMB = 2,5-diisocyano-2,5-dimethylhexane), this excitation is followed by a very efficient intersystem crossing to the $^3A_{2u}$ triplet state.[11] As in the analogous and very well-studied Pt complex PtPOP,[12−16] population of the bonding orbital located between the two metal centers is expected to lead to a contraction along the metal−metal axis as also directly observed in $Rh_2(dimen)_4^{2+}$.[6]

The present work reports time-resolved X-ray scattering measurements of the structural changes due to electronic excitation of $Ir_2(dimen)_4^{2+}$ in acetonitrile solution. As demonstrated in previous work,[17,18] structural modeling and analysis of difference scattering signals can give detailed insight into the photoinduced structural changes and kinetics. In addition, special emphasis will be given to determining the ground-state structure of $Ir_2(dimen)_4^{2+}$ in solution from the X-ray scattering data.

EXPERIMENTAL SECTION

Methods. The experiments reported in this work were all carried out at beamline ID09B at the European Synchrotron Radiation Facility (ESRF, Grenoble, France) using the well-established 986.3 Hz laser pump/X-ray probe protocol with 2 ps 390 nm laser pulses and pink-beam X-ray energy spectrum with an intensity maximum at 18.25 keV.[17,18] A solution of $Ir_2(dimen)_4^{2+}$ (6 mM) in acetonitrile was constantly circulated through a fast-flowing liquid-jet setup, ensuring complete sample replacement between each pump−probe cycle. Data were analyzed using the structural fitting approach previously used for this class of experiments and previously described in detail,[15,19,20] in this work using DFT-derived structures as the starting point for analysis.

Synthesis. $Ir_2(dimen)_4^{2+}$ was synthesized onsite by direct mixing of 1,8-diisocyano-paramenthane (dimen) and $Ir_2Cl_2(COD)_2$ (COD = 1,5-cyclooctadiene) in a 4:1 ratio in acetontrile rigorously purged with argon. The 6 mM solution displayed an intense dark purple color. The typical solution volume for one experiment was 150 mL. Under deoxygenized conditions the $Ir_2(dimen)_4^{2+}$ solution was observed to be very robust under laser and X-ray irradiation with only minor sample decay over long periods (12 h) of near-constant exposure to laser and X-ray pulses. The sample volume was constantly monitored for loss due to evaporation (~10 mL/4 h) and kept constant by topping up with Ar-purged acetonitrile.

Experimental Setup. Details of the experimental setup at ESRF beamline ID09B for time-resolved studies are given elsewhere[17] but are briefly reviewed here. Individual ~100 ps long X-ray pulses from the u17 undulator were selected by means of a high-speed mechanical chopper with a 265 ns opening time, sufficient to isolate X-ray bursts from the individual electron bunches in several of the ESRF filling modes.[21] Thereby the frequency of X-ray pulses arriving at the sample was reduced to 986.3 Hz (360th subharmonic of the synchrotron orbit frequency). A Ti:sapphire amplified femtosecond laser with a 780 nm fundamental wavelength was phase locked to the same 986.3 Hz frequency. For the experiments reported here, the 780 nm pulses were frequency doubled to 390 nm in a BBO crystal and stretched to 2 ps by passing through two fused silica prisms, the latter in order to reduce two-photon excitation events. Spatial overlap between the laser and X-ray beams at the sample position was attained using a pinhole, with the laser beam incident at a 10° angle to the X-ray beam and focused to a 120 μm diameter spot size. A corresponding X-ray focus of 100 μm × 60 μm ($w \times h$) was obtained with a Pt-coated toroidal mirror, also used for rejecting higher harmonics of the undulator spectrum. This renders the X-ray energy spectrum quasi-monochromatic with a triangular energy profile peaking at 18.25 keV (9 mm gap) and 4.5% bandwidth. Absolute timing of the laser and X-ray pulses was measured with a fast GaAs photodiode. Subnanosecond changes in the arrival time of the laser pulses at the sample position were controlled by shifting the phase of the laser oscillator feedback loop. Timing jitter was better than 5 ps.

The sample solution was continuously circulated through a sapphire nozzle, producing a stable liquid film with 300 μm thickness at the laser/X-ray overlap position and a flow speed of ~4 m/s, ensuring complete sample replacement between each pump−probe cycle. An Ar-filled chamber protected the liquid jet from exposure to atmospheric oxygen, and the sample reservoir was likewise protected by continuous purging by Ar saturated with acetonitrile vapor.

Scattered X-rays were collected on a 2048 × 2048 FReLoN CCD detector, integrating 2000 X-ray pulses for each image, corresponding to ~2 s exposure time. Scattering images were subsequently corrected for polarization of the X-ray beam, solid angle coverage, and the angle-dependent absorption efficiency of the detector before being azimuthally integrated to give 1-dimensional scattering curves $S(2\theta)$. For clarity of presentation but not used in the analysis, all scattering angles were converted to scattering vectors $Q = (4\pi \sin(2\theta/2))/\lambda$, with λ being the X-ray wavelength and using a weighted average corresponding to the undulator spectrum $I(\lambda)$. For the experiments reported here, scattering

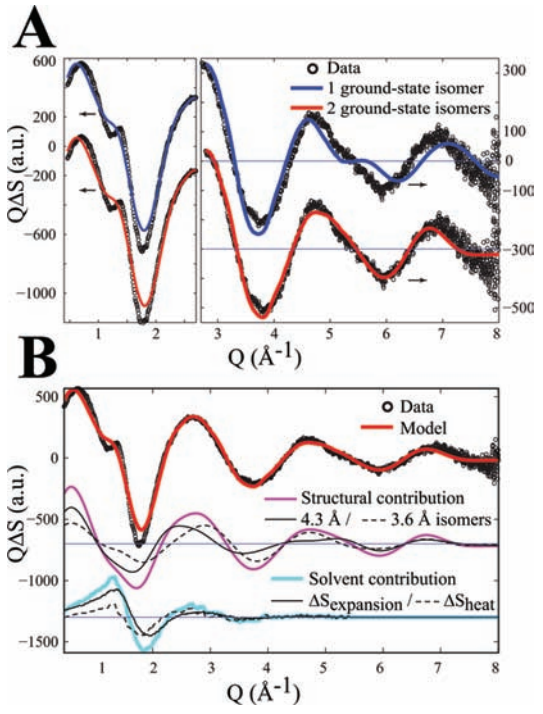

Figure 2. (A) Results of fitting structural models incorporating one (blue line) and two (red line) ground-state structures in the simulated difference scattering signal fit to the acquired difference signal $\Delta S(Q)$ at $\Delta t = 30$ ns. A very significant improvement in the quality of the fit at $Q > 3$ Å^{-1} is observed when two possible ground-state structures are used. (B) Partitioning of the best-fit model simulation into the contribution from structural changes in the solute (magenta) and solvent (blue). These are further partitioned into contributions from the structural changes in the long (full) and short (dashed) isomers as well as contributions due to expansion (full line) and heating (dashed line) of the solvent.

patterns were acquired in sequences of 4−5 images with the laser pulse arriving at predetermined time intervals $\Delta t \equiv t_{probe} - t_{pump}$ before the center of the X-ray pulse (positive delay, "Laser-on"), with such sequences separated by individual reference images (also 2 s integration time) where the laser pulse arrived after the X-ray pulse (negative delay, "Laser-off"). For each time delay, 100−200 images were acquired.

Difference scattering signals were constructed by first scaling the high-Q part of the individual scattering curves to the calculated coherent + incoherent molecular scattering from a "liquid unit cell" representing the stoichiometry of the solution. From each scattering curve with a positive delay Δt, the average of the two nearest laser-off curves was then subtracted to form the difference signal, $\Delta S(Q)$. For each time delay Δt, the 100−200 individual $\Delta S(Q)$ curves were subsequently analyzed and statistically significant outliers removed by successive point-by-point and ensemble application of the Chauvenet Criterion.[18,22] The outliers constituted on the order of 1% of the curves. The final step in the preanalysis was construction of averaged $\Delta S(Q)$ curves for each time delay, Figure 2A showing one such curve. The noise level $\sigma(Q)$ for each curve was estimated from the residual of local (20 points) fit to low-order (second) polynomials.[18,23]

DFT Calculation of Starting-Point Structures. To provide starting structures for the structural analysis described in detail below, several DFT calculations were performed. All calculations were carried out in the ORCA framework[24] with the one-parameter hybrid version of the Perdew−Burke−Erzerhoff functional with 25% HF exchange (PBE0). In earlier work Adamo et al. demonstrated successful use of the PBE0 hybrid functional for transition-metal complexes.[25] The Gaussian-type Ahlrichs double-ζ basis set (DZ) was used in all calculations, and COSMO was used to include electrostatic interactions with the acetonitrile solvent. Def2-triple-ζ Stuttgart−Dresden effective core potentials (ECP[Ir=def2-TZVP])[26,27] were used for the Ir atoms to reduce the computation time. Ground-state calculations were done using restricted Kohn−Sham (RKS) method, and the excited-state calculations were done for the triplet by setting the spin multiplicity to 3 and doing unrestricted Kohn−Sham (UKS) calculations. For all four structural isomers, DFT calculations uniformly favor a ground state with d_{IrIr} = 4.6−4.9 Å located in a very shallow Ir−Ir potential when no structural or symmetry restrictions are imposed.

Data Analysis. Analysis of the difference scattering signals shown in Figure 2A followed the general methodology described in detail in our previous work[18] except for treatment of the solvent response and determination of the solution ground-state structure of $Ir_2(dimen)_4^{2+}$. Turning first to the solvent response, the laser pump leads to impulse heating and subsequent expansion of the solvent due to ultrafast release of excess vibrational energy from the excited solute molecules.[28] The contribution from these effects to the difference scattering signal can be included through the use of previously determined solvent differentials[15,28] or through molecular dynamics simulations.[17] However, such data were not available for the present study, and instead, the immediate (<100 ps, heating $\Delta S_{\Delta T}$) and long-term (>10 ns, expansion-dominated $\Delta S_{\Delta\rho}$) response of the solvent were determined in another set of experiments using a chemically inert chromophore as in the recent work reported by Salassa et al.[29] and detailed in the Supporting Information. Figure 2B, lower part, shows these two solvent contributions to the difference scattering signal.

Turning next to determination of the solution ground-state structure, the spectroscopic evidence presented by Exstrom et al.[7] indicates the presence of not one but two distinct solution-state structures characterized by different Ir−Ir distances. To provide a basis for structural analysis, DFT calculations of the electronic and geometric structure of $Ir_2(dimen)_4^{2+}$ were carried out within the ORCA framework as described above.

Structural information was obtained by fitting[18] a simulated difference signal ΔS_{Sim} to the acquired difference signal ΔS_{Data} for a given time delay Δt while varying the excitation fraction α and a set of n structural parameters P_n. The scattering is calculated through the (orientation-averaged) Debye expression for the molecular form factor

$$S(Q) \propto F_{mol}^2(Q) = \sum_{\substack{i,j,k \\ i<j}}^{N} f_i f_j \frac{\sin(Qr_{ij})}{Qr_{ij}} + |f_{kk}|^2 \qquad (1)$$

Here, f_i is the atomic form factor for atom i and r_{ij} is the distance between atoms i and j. Introducing the excitation fraction α, the structural part of the simulated difference signal is given by $\alpha\Delta S_{Sim,struct} = \alpha(S_{On} - S_{Off}) = (\alpha S^n_{Exc} + (1 - \alpha)S_{Ground}) - S_{Ground}$, with the superscript n denoting the nth set of structural parameters. To accurately fit the experimental data, the solvent contribution is included such that the full time-dependent simulated signal is given by

$$\begin{aligned}\Delta S(Q)_{Sim} &= \alpha\Delta S(Q)_{Sim,\,struct} + \Delta S(Q)_{Solv} \\ &= \alpha\Delta S(Q)_{Sim,\,struct} + \alpha_{\Delta T}\Delta S(Q)_{\Delta T} \\ &\quad + \alpha_{\Delta\rho}\Delta S(Q)_{\Delta\rho} \end{aligned} \qquad (2)$$

In this expression, $\Delta S(Q)_{\Delta T}$ and $\Delta S(Q)_{\Delta\rho}$ are the difference signal responses to, respectively, solvent heating and subsequent expansion, as described above. $\alpha_{\Delta T}$ and $\alpha_{\Delta\rho}$ are the corresponding scaling factors.

dx.doi.org/10.1021/ic2006875 |Inorg. Chem. 2011, 50, 9329–9336

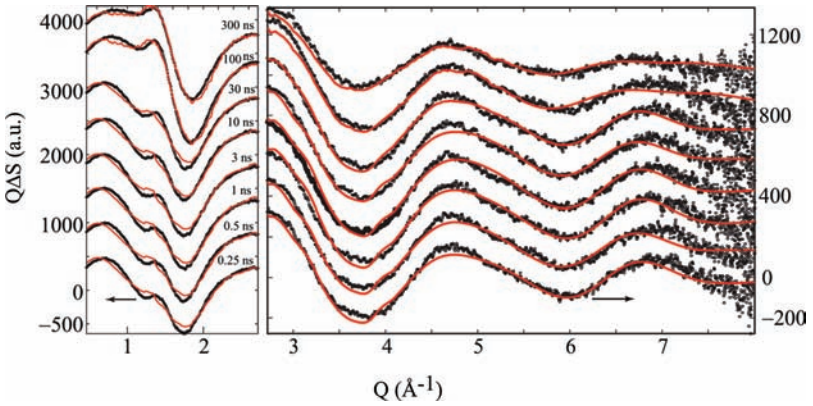

Figure 3. Data (black points) and best-fit models (red lines) for the eight investigated time steps from 250 ps to 300 ns after excitation. Good agreement between data and simulations is observed for all time delays, in particular for $Q > 3$ Å^{-1}. The comparatively poor fit around $Q = 1.5$ Å^{-1} is most pronounced at short time delays, where the difference signal in this region is dominated by the change in scattering due to solvent heating, cf. Figure 4. The noise level $\sigma(Q)$ is reflected by the local scatter in the data points.

The fit is evaluated through minimizing a χ^2 estimator[30]

$$\chi^2 = \sum_N \frac{(\Delta S_{\mathrm{Sim}} - \Delta S_{\mathrm{Data}})^2}{\sigma^2}/(N - P - 1) \quad (3)$$

where N is the number of data points, σ the experimental uncertainty at each point, and P the number of free parameters in the model. The χ^2 value for each possible set of parameters can be associated with a relative likelihood L defined as $L_{p_n} \propto \exp(-\chi^2/2)$.

Figure 2A shows in blue the result of such a fit, taking as starting points DFT-derived structures for the triplet excited state and ground state, with minimum energy Ir−Ir separations of 2.88 Å and 4.68 Å, respectively. To allow for differences between the calculated and the actual molecular structures, the Ir−Ir separation was further varied from 2.5 to 3.5 Å for the excited state and from 3 to 5.5 Å for the ground-state structure, keeping all other structural parameters constant. As is evident from Figure 2A, the resultant fit (blue line) to the data is not satisfactory.

A better fit was obtained assuming two coexisting ground-state structures as deduced from spectroscopy by Exstrom et al.[7] Figure 2A shows in red the result of fitting a model accommodating two ground-state structures that differ in the Ir−Ir distance. The structural part of the expanded model is quantitatively given by $\Delta S_{\mathrm{Sim,struct}} = \beta\Delta S_{\mathrm{short}} + (1 - \beta)\Delta S_{\mathrm{long}}$, where both the long and the short Ir−Ir distances are allowed to vary independently as is the partitioning β among the two contributions. Thus, the goodness-of-fit measure χ^2 and the likelihood L are functions of the three Ir−Ir distances $d_{\mathrm{IrIr}}^{\mathrm{GS1}}$, $d_{\mathrm{IrIr}}^{\mathrm{GS2}}$, and $d_{\mathrm{IrIr}}^{\mathrm{ES}}$, the partitioning β, and the three α parameters introduced above

$$\chi^2 = \chi^2(d_{\mathrm{IrIr}}^{\mathrm{GS1}}, d_{\mathrm{IrIr}}^{\mathrm{GS2}}, d_{\mathrm{IrIr}}^{\mathrm{ES}}, \beta, \alpha_{\mathrm{exc}}, \alpha_{\Delta T}, \alpha_{\Delta\rho}) \quad (4)$$

From the seven-dimensional likelihood space, the most-likely set of parameter values, their uncertainties, and their correlations can be determined.[18]

DFT-optimized structures with Ir−Ir distances of 2.9 Å in the excited state and 3.5 and 4.3 Å in the two ground-state isomers were used as starting points for the fitting procedure (see Supporting Information for details). When fitting to the scattering data, the Ir−Ir distances were allowed to vary freely around the initial guess while the ligand structure was kept rigid. It is noted that while this structural variation gives a good estimate of the scattering signal, it does not accurately capture the overall structure of the molecules in question, as the Ir−Ir distance is known to be strongly coupled to both pyramidal deformation of the square-planar isocyanide end groups and the dihedral C−Ir−Ir−C ligand twist angle.[7] As Figure 2A shows, application of the "two-isomer" model results in a significantly better fit.

RESULTS

The analysis strongly indicates that the difference scattering signal acquired 30 ns after laser excitation of $Ir_2(dimen)_4^{2+}$ in acetonitrile can be interpreted through a structural analysis incorporating one population of excited-state $Ir_2(dimen)_4^{2+}$ with a single well-defined Ir−Ir bond length and two ground-state populations with significantly longer Ir−Ir distances. From the maximum likelihood analysis we arrive at an excited-state Ir−Ir distance of 2.90(2) Å and ground-state distances of 3.60(9) and 4.3(1) Å. The excitation fraction α is determined as 9.7(5)% and the ground-state partitioning parameter β as 0.54(7). The cited 1-σ confidence intervals are conservative and incorporate all correlations between the fit parameters.

To further investigate the excited-state structure and related dynamics of the photoexcited $Ir_2(dimen)_4^{2+}$ system, Figure 3 shows difference signals and best fits for the eight time delays from 250 ps to 300 ns. Very good agreement between data and simulations is observed in the high-Q part of the signal for all time delays, although an inability of the simulations to capture the sharp features at $Q = 1-2$ Å^{-1} is noticed. We attribute this to a necessary smoothing of the temperature-related solvent contribution (see Supporting Information) and the choice not to include the ligand twist as a fit parameter, two features of our model expected to be most consequential in the low-Q part of the difference scattering signal.

Figure 4A shows the temporal evolution of the excitation fraction (black circles) and an exponential fit to this time series. A best-fit lifetime of 410(70) ns is obtained. Also shown in this figure are the scaling factors $\alpha_{\Delta T}$ (red) and $\alpha_{\Delta\rho}$ (blue) for the two solvent contributions. The initial temperature increase within the first 100 ps is followed by cooling on the 10−100 ns time scale concomitant with solvent expansion (density decrease, $-\alpha_{\Delta\rho}$), in accordance with the expected hydrodynamics.[28] Figure 4B illustrates the obtained best-fit values of the four parameters related to structure. Essentially no time dependence up to 100 ns is observed, at which point there is a decrease in the partitioning fraction β, suggesting faster relaxation to the short-distance isomer. This change in partitioning is associated with a slight increase in the best-fit values for the ground-state Ir−Ir distances, suggesting a more elaborate model is needed to fully describe the structural dynamics at long time delays as discussed further below.

dx.doi.org/10.1021/ic2006875 |Inorg. Chem. 2011, 50, 9329–9336

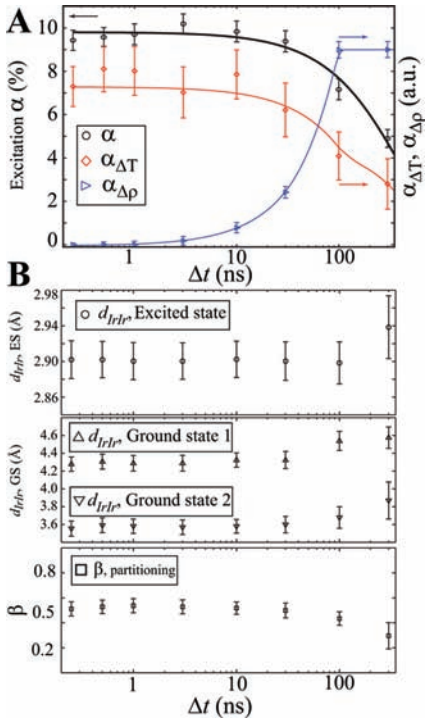

Figure 4. (A) Excitation fraction (black circles) for the best-fit models as a function of time delay Δt. The observed excitation fraction is well fitted by a single-exponential decay with lifetime τ = 410 ns (black line). Red and blue points show the hydrodynamic scaling factors $\alpha_{\Delta T}$ and $\alpha_{\Delta\rho}$. A fast initial increase $\alpha_{\Delta T}$ due to impulse heating is followed by cooling and expansion on the 10−100 ns time scale. The red and blue lines are interpolations of the data points to illustrate the temporal evolution. (B) Structural parameters for the best-fit models as a function of time delay. These appear essentially independent of the time delay, with an excited-state Ir−Ir distance of 2.90 Å. The best-fit ground-state structures have d_{IrIr} = 3.6 and 4.3 Å for the short- and long-distance isomer, respectively. The lower panel illustrates the ground-state partition fraction, with the two isomers present in equal amounts for all but the longest time delays.

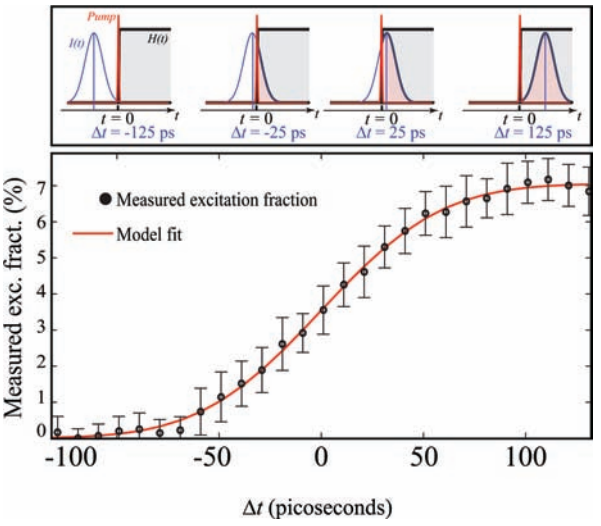

Figure 5. Schematic depiction of the slicing methodology and measured excitation fraction as a function of time delay Δt (black circles). Assuming instantaneous formation of the excited state on the 10 ps time scale, the red line is a fit of a broadened step function, eq 6, to the excitation fraction. The quality of the fit supports the model assumptions of instantaneous formation and no excited-state depopulation at the investigated time scale.

Figure 5 presents a 10-ps time-slicing study aimed at investigating the excited-state structure at shorter time scales. The arrival time of the 2 ps laser pulse on the sample was gradually moved through the ∼100 ps long X-ray pulse with temporal envelope $I(t)$. On the 10 ps time scale, the structural change due to the excitation pulse can be considered instantaneous. In the limit of infinitely short pump and probe pulses (omitting the Q dependence to simplify the notation), the expected signal can thus be represented as the signal due to the instantaneous structural change, ΔS_{Inst}, multiplied by a heaviside step function $H(t)$ centered at t = 0, $\Delta S(t) = H(t)_{\Delta t=0}\Delta S_{\mathrm{Inst}}$. Representing the finite length of the probe pulse as a Gaussian intensity profile of width σ_{p}, the experimental scheme is depicted in the top panel of Figure 5. The time delay is calculated from the arrival time of the midpoint of the pulses and referenced to the arrival time of the pump pulse. In the present case the arrival time of the laser pump pulse at the sample position is defined to be t_{pump} = 0. Considering all possible values of the time delay $\Delta t \equiv t_{\mathrm{probe}} - t_{\mathrm{pump}}$, the measured difference signal can now be written as the convolution of the step function and the intensity profile

$$\Delta S(\Delta t) \propto \int_{-\infty}^{\infty} \mathrm{d}t \Delta S_{\mathrm{Inst}} H(t)_{\Delta t=0} I(t) \tag{5}$$

Introducing $I(t) = (1/(2\pi\sigma_{\mathrm{p}})^{1/2})\exp(-((t-\Delta t)^2)/(2\sigma_{\mathrm{p}}{}^2))$ and substituting $t' = t - \Delta t$ this integral can be solved to give

$$\Delta S(\Delta t) \propto 1 + \mathrm{erf}\left(\frac{\Delta t}{\sqrt{2}\sigma_{\mathrm{p}}}\right) \tag{6}$$

Comparing with the top part of Figure 5, this expression is recognized as the integral of the probe pulse from the point of intersection with the pump pulse to infinity. Referring to eq 2, the signal from the structural change $\Delta S_{\mathrm{Struct}}$ is linear in the excitation fraction α, and from the expressions above, the measured excitation fraction from the structural analysis of the difference scattering signal at each time delay would be expected to follow the form of eq 6. Figure 5 shows the excitation fraction α (black circles) as a function of the nominal time delay Δt. In this analysis, only the excitation fraction, the temperature increase, and the excited-state Ir−Ir bond length (α_{exc}, $\alpha_{\Delta T}$, and $d_{\mathrm{IrIr}}^{\mathrm{ES}}$ in eq 3) were allowed to vary in the structural fitting. The red line in Figure 5 is a fit of eq 6 to the data points, and excellent agreement between data and fit is observed. From the analysis we recover a probe pulse length $l_{\mathrm{p}} = 2.35\sigma_{\mathrm{p}}$ of 110(10) ps, in good agreement with published ESRF values for the 4-bunch filling mode. Carrying out the same analysis for the prefactor of the heating contribution to the scattering signal, $\alpha_{\Delta T}$, we obtain essentially the same result for the probe pulse length, l_{p} = 100(30) ps.

The lifetime of the singlet excited state has been determined from transient spectroscopy (see Supporting Information) to be ∼65 ps, shorter than the probe pulse duration but longer than the effective time resolution of the time-slicing method. The demonstrated slicing scheme thus offers an opportunity to investigate

dx.doi.org/10.1021/ic2006875 |Inorg. Chem. 2011, 50, 9329–9336

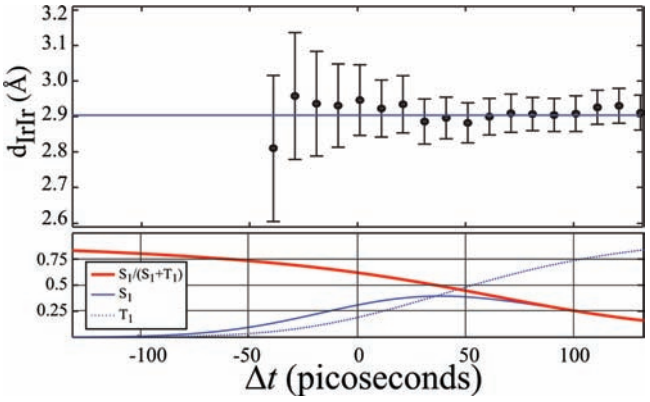

Figure 6. (Top) Ir−Ir distance measured as a function of time delay Δt. For $\Delta t < -40$ ps ($\alpha_{Eff} < 1\%$) no reliable estimate of the distance could be obtained. The blue line represents the result of the longer time scales study. (Bottom) Relative fractions of the singlet (full) and triplet (dashed) excited state probed by the 100 ps long X-ray pulse as a function of time delay. (Red line) Relative strength of the singlet contribution to the difference signal, which dominates until $\Delta t = 0$ ps. Any change in the Ir−Ir separation related to the singlet−triplet transition is at the limit of detection, but a slight shortening of the Ir−Ir bond is suggested.

any structural change accompanying the singlet−triplet electronic transition. If the singlet state is assumed to undergo intersystem crossing to the triplet state with unity efficiency we can write

$$\Delta S_{S_1}(\Delta t) \propto \int_{-\infty}^{\infty} dt \Delta S_{inst} H(t) \exp\left(\frac{-t}{\tau}\right) I(t) \quad (7)$$

$$\Delta S_{T_1}(\Delta t) \propto \int_{-\infty}^{\infty} dt \Delta S_{inst} H(t) \left[1 - \exp\left(\frac{-t}{\tau}\right)\right] I(t) \quad (8)$$

where the dependence on Δt is contained in $I(t)$ as above. These convolution integrals can again be solved analytically to give

$$\Delta S_{S_1}(\Delta t) \propto -\exp\left(\frac{\sigma^2 - 2\Delta t\tau}{2\tau^2}\right) \times \left(1 - \mathrm{erf}\left(\frac{\sigma^2 - \Delta t\tau}{\sqrt{2}\sigma\tau}\right)\right) \quad (9)$$

$$\Delta S_{T_1}(\Delta t) \propto \left(1 + \mathrm{erf}\left(\frac{\Delta t}{\sqrt{2}\sigma}\right)\right) - \exp\left(\frac{\sigma^2 - 2\Delta t\tau}{2\tau^2}\right) \times \left(1 - \mathrm{erf}\left(\frac{\sigma^2 - \Delta t\tau}{\sqrt{2}\sigma\tau}\right)\right) \quad (10)$$

To relate this to the relative signal strengths from the singlet and triplet excited-state populations of $Ir_2(dimen)_4^{2+}$, the bottom panel in Figure 6 shows in blue eqs 9 and 10 as calculated for τ_{S1} = 63 ps and l_p = 110 ps. The red line illustrates the contribution to the difference signal ΔS from the singlet population relative to the triplet population as a function of time delay. From this it is clear that at nominal time delays Δt earlier than $\Delta t = 0$ the measured difference signal is dominated by the singlet excited state. The top part of Figure 6 shows the result of fitting the excited-state Ir−Ir separation for each time delay beyond $\Delta t = -40$ ps, corresponding to an "effective" probed excitation fraction exceeding ~1%. At $\Delta t = -10$ ps the signal strength allows determination of d_{IrIr} with reasonable accuracy. Taking a five-point uncertainty-weighted average around this time delay, where the singlet still dominates the signal, leads to d_{IrIr} = 2.93(2) Å. This can be compared with a similar five-point average for the five points at Δt = 90−140 ps, where d_{IrIr} = 2.91(1) Å is obtained. Thus, from these data no significant shift in Ir−Ir separation is observed as the signal gradually becomes dominated by the triplet excited-state population. However, it is evident that even in this experiment with comparatively few repetitions (108 exposures/time delay) and thus a relatively poor S/N ratio for each time step kinetics and structural changes can be followed with a time resolution significantly better than the ~100 ps given by the probe pulse. Thus, this methodology is paving the way for new classes of experiments.

DISCUSSION

Determination of the excited-state structure of $Ir_2(dimen)_4^{2+}$ with a 2.9 Å separation between the two Ir atoms in the triplet excited state represents an exceptionally large structural rearrangement due to photoexcitation. We interpret our observations in the framework derived by Miskowski et al.,[3] where the metal atoms in the ground state exist on a very shallow ligand-dominated potential surface along the M−M coordinate. Upon excitation, the bonding orbital between the two Ir atoms becomes populated, effectively enhancing the attractive interaction between the two metal atoms, which changes the potential to a steeper and more metal-dominated configuration with a significantly shorter metal−metal equilibrium distance. From steady-state crystallographic data for both $Ir_2(dimen)_4^{2+}$ and $Rh_2(dimen)_4^{2+}$, short M−M distances in these compounds are accompanied by both a torsional twist of the ligand system and pyramidal distortion of the isocyanide conformation around the metal centers. We ascribe the observed difference between the present results and earlier diffraction work[6] on the excited-state structure of the analogue $Rh_2(dimen)_4^{2+}$ system to hindering of these secondary deformation mechanisms due to crystal packing forces. However, the effect of these appears significantly less pronounced in the excited state than for the ground-state structures, in accordance with the much shallower metal−metal potential in the ground state.

While already suggested by Exstrom et al. in 1996, the possible coexistence of at least two different structural isomers of $Ir_2(dimen)_4^{2+}$ in acetonitrile solution has led to very little discussion in the literature and was never confirmed until very recent ultrafast transient absorption experiments.[10] Exstrom et al. discussed the solution-state spectra in terms of bond-stretch isomerism and associated the spectroscopic features in the solution state data to ground-state populations with Ir separations of 4.4 and 3.6 Å, respectively. Although not supported by our DFT calculations, this part of our interpretation is in good agreement with the hypothesis of more than one ground-state structure. The almost exact 50/50 partitioning between the long and short distance populations also determined in the present study suggests an explanation. As discussed in the 1990 work by A. Sykes et al.,[8] the asymmetric geometry of the dimen ligand allows for the possible coexistence of four structural isomers being present both in solution and in crystals. In the latter case, this leads to ligand disorder in structural refinements from

dx.doi.org/10.1021/ic2006875 |Inorg. Chem. 2011, 50, 9329–9336

crystallographic data. From statistical arguments, one of these isomers, the 1:3 isomer with one ligand having the ring near one Ir atom and the other three ligands having the ring oriented toward the second Ir atom, should have an abundance of 1/2, whereas the other isomers have abundances of 1/4 (2:2-*cis*) and 1/8 (both 2:2-*trans* and 4:0 isomer). The optical excitation pulse at 390 nm addresses a position in the absorption spectra where the absorption is equal for all isomers. On the basis of the statistical abundances of the four isomers and our result of $\beta = 0.5$, we tentatively assign either the long (4.3 Å) or the short (3.6 Å) Ir−Ir distance to the 1:3 isomer. This suggestion of a direct connection between head/tail ligand arrangements and Ir−Ir distance does not disagree with analysis of the ultrafast spectroscopy data presented by Hartsock et al.[10] However, further work incorporating, e.g., the temperature dependence of the spectroscopic features or X-ray investigations of the ground-state solution scattering at different temperatures will be needed to distinguish between the models proposed. This work is under way.

While the 10 ps time resolution results presented above do not imply any significant structural change related to the electronic singlet−triplet transition in $Ir_2(dimen)_4^{2+}$, the data shown demonstrate the feasibility of this type of study. Further studies along this line of inquiry would benefit from data obtained with lower bunch-charge filling patterns in the synchrotron, where X-ray intensity is sacrificed for shorter pulse lengths, as this would effectively sharpen the probed population distributions depicted in blue in Figure 4A.

CONCLUSIONS

In the present study, time-resolved liquid-state X-ray scattering has been utilized to demonstrate remarkable bond shortening in $Ir_2(dimen)_4^{2+}$ in acetonitrile following photoexcitation by short laser pulses at 390 nm. From an analysis incorporating two ground-state structures differing significantly in the Ir−Ir separation, the difference scattering signals were found to be very well described by a contraction in Ir−Ir distance from 3.60(9)/4.3(1) to 2.90(2) Å upon population of the pσ orbital. This corresponds to 1.4 Å contraction of the Ir−Ir distance in the case of the long-distance isomer. Such a dramatic reduction in Ir−Ir distance is significantly greater than the contraction observed in crystal studies of the analogous Rh compound $Rh_2(dimen)_4^{2+}$.[6] We ascribe this difference to the absence of crystal packing forces in the present solution-state study. From the analysis of eight time delays in the range from 250 ps to 300 ns, the lifetime of the triplet excited state has been determined to be 410(70) ns, with the possibility of differing lifetimes between the two structural isomers included in the model description noted.

A second study demonstrated a 5−10-fold improvement of the effective time resolution of the chopper-based setup at ESRF beamline ID09B beyond the intrinsic ~100 ps width of the probe pulse. Gradually shifting the temporal position of the laser pump pulse within the X-ray probe pulse in 10 ps steps allowed the fraction of excited-state solute molecules probed by the X-ray pulse to be monitored with good accuracy as a function of sub-100 ps time delay. From analysis of this "effective excitation fraction" as a function of pump−probe delay, the reported fwhm X-ray pulse width of the ESRF in 4-bunch mode was recovered. Independent analysis of the solvent heating signal confirmed the feasibility of the method. Analysis of the Ir−Ir bond length as a function of time delay on the sub-100 ps time scale was inconclusive but suggested a slight shortening of the bond upon intersystem crossing from the singlet to the $^3A_{2u}$ triplet state. Ten picosecond time resolution appears feasible, paving the way for studying new classes of phenomena.

In summary, the present study has determined the excited-state Ir−Ir distance of $Ir_2(dimen)_4^{2+}$ in acetonitrile to be 2.90(2) Å and confirmed the existence of at least two structural isomers present in the ground state. Further investigations of this system will utilize different excitation wavelengths and temperature-dependence studies to elucidate the structural isomerism in this system.

ASSOCIATED CONTENT

Supporting Information. The supplementary online information includes information on the difference-signal contributions from impulsive solvent heating, details of the data analysis approach, transient absorption data and further details of the 10 ps time slicing experiment. This material is available free of charge via the Internet at http://pubs.acs.org.

AUTHOR INFORMATION

Corresponding Author
*E-mail: hald@risoe.dtu.dk.

ACKNOWLEDGMENT

The authors are grateful for computer resource allocation and discussion of the DFT results with Stephan Sauer and Casper Steinmann, both Chemistry Department, University of Copenhagen. The assistance of K. Bechgaard, P. Hammershøj, and T. Just (Chemistry Department, University of Copenhagen) with the synthesis work is very much appreciated. The assistance of S. Canton (Maxlab, Sweden) with the transient optical measurements performed at CNM, Argonne National Laboratory, is gratefully acknowledged. This work was supported by the Danish National Research Foundation's Centre for Molecular Movies and DANSCATT

REFERENCES

(1) Lewis, N. S.; Mann, K. R.; Gordon(II), J.; Gray, H. B. *J. Am. Chem. Soc.* **1976**, *98:23*, 7461–7463.
(2) Lewis, N. S.; Mann, K. R.; Gordon(II), J.; Gray, H. B. *J. Am. Chem. Soc.* **1977**, *99:16*, 5525–5526.
(3) Miskowski, V. M.; Rice, S. F.; Gray, H. B.; Dallinger, R. F.; Milder, S. J.; Hill, M. G.; Exstrom, C. L.; Mann, K. R. *Inorg. Chem.* **1994**, *33*, 2799–2807.
(4) Harvey, P. D. *Coord. Chem. Rev.* **2001**, *219−221*, 17–52.
(5) Novozhilova, I. V.; Volkov, A. V.; Coppens, P. *Inorg. Chem.* **2004**, *43*, 2299–2307.
(6) Coppens, P.; Gerlits, O.; Vorontsov, I.; Kovalevsky, A.; Chen, Y.; Graber, T.; Gembicky, M.; Novozhilova, I. *Chem. Commun.* **2004**, *19*, 2144–2145.
(7) Exstrom, C. L.; Britton, D.; Mann, K. R.; Hill, M. G.; Miskowski, V. M.; Schaefer, W. P.; Gray, H. B.; Lammana, W. M. *Inorg. Chem.* **1996**, *35*, 549–550.
(8) Sykes, A. G.; Mann, K. R. *J. Am. Chem. Soc.* **1990**, *112*, 7247–7254.
(9) Sykes, A. G.; Mann, K. R. *Inorg. Chem.* **1990**, *29*, 4449–4453.
(10) Hartsock, R. W.; Zhang, W.; Hill, M. G.; Sabat, B.; Gaffney, K. J. *J. Phys. Chem. A* **2011**, *115*, 2920–2926.
(11) Miskowski, V. M.; Rice, S. F.; Gray, H. B.; Milder, S. J. *J. Phys. Chem.* **1993**, *97*, 4277–4283.

(12) Rice, S. F.; Gray, H. B. *J. Am. Chem. Soc.* **1983**, *105*, 4571–4575.
(13) Kim, C. D.; Pillet, S.; Wu, G.; Fullagar, W.; Coppens, P. *Acta Crystallogr., Sect. A* **2001**, *A58*, 133–137.
(14) Novozhilova, I.; Volkov, A.; Coppens, P. *J. Am. Chem. Soc.* **2002**, *125*, 1079–1087.
(15) Christensen, M.; Haldrup, K.; Bechgaard, K.; Feidenhans'l, R.; Kong, Q.; Cammarata, M.; Russo, M. L.; Wulff, M.; Harrit, N.; Nielsen, M. M. *J. Am. Chem. Soc.* **2009**, *131*, 502–508.
(16) van der Veen, R. M.; Milne, C. J.; Nahhas, A. E.; Lima, F. A.; Pham, V.-T.; Best, J.; Weinstein, J. A.; Borca, C. N.; Abela, R.; Bressler, C.; Chergui, M. *Angew. Chem., Int. Ed.* **2009**, *48*, 2711–2714.
(17) Kim, T. K.; Lee, J. H.; Wulff, M.; Kong, Q.; Ihee, H. *ChemPhysChem* **2009**, *10*, 1958–1980.
(18) Haldrup, K.; Christensen, M.; Nielsen, M. M. *Acta Crystallogr., Sect. A* **2010**, *A66*, 261–260.
(19) Haldrup, K.; Christensen, M.; Cammarata, M.; Kong, Q.; Wulff, M.; Mariager, S. O.; Bechgaard, K.; Feidenhans'l, R.; Harrit, N.; Nielsen, M. M. *Angew. Chem., Int. Ed.* **2009**, *48*, 4180–4184.
(20) Christensen, M.; Haldrup, K.; Kjær, K. S.; Cammarata, M.; Wulff, M.; Bechgaard, K.; Weihe, H.; Harrit, N. H.; Nielsen, M. M. *Phys. Chem. Chem. Phys.* **2010**, *12*, 6921–6923.
(21) Cammarata, M.; Eybert, L.; Ewald, F.; Reichenbach, W.; Wulff, M.; Anfinrud, P.; Schotte, F.; Plech, A.; Kong, Q.; Lorenc, M.; Lindenau, B.; Raebiger, J.; Polachowski, S. *Rev. Sci. Instrum.* **2009**, *80*, 124505-1–124504-9.
(22) Taylor, J. R. *Introduction to Error Analysis*; University Science Books, 1997.
(23) Dent, A.; Stephenson, P.; Greaves, G. *Rev. Sci. Instrum.* **1991**, *63*, 856–852.
(24) http://www.thch.uni-bonn.de/tc/orca/.
(25) Adamo, C.; Barone, V. *Theor. Chem. Acc.* **2000**, *105*, 169–172.
(26) Andrae, D.; Haussermann, U.; Dolg, M.; Stoll, H.; Preuss, H. *Theor. Chim. Acta* **1991**, *78*, 247–266.
(27) Weigend, F.; Ahlrichs, R. *Phys. Chem. Chem. Phys.* **2005**, *7*, 3297–3305.
(28) Cammarata, M.; Lorenc, M.; Kim, T.; Lee, J. H.; Kong, Q. Y.; Pontecorvo, E.; Russo, M. L.; Schiro, G.; Cupane, A.; Wulff, M.; Ihee, H. *J. Chem. Phys.* **2006**, *124* (124504), 1–9.
(29) Salassa, L.; Borfecchia, E.; Ruiu, T.; Garino, C.; Gianolio, D.; Gobetto, R.; Sadler, P. J.; Cammarata, M.; Wulff, M.; Lamberti, C. *Inorg. Chem.* **2010**, *49*, 11240–11248.
(30) Press, W. H.; Flannery, B. P.; Teukolsky, T. A.; Vetterling, W. T. *Numerical Recipes-The Art of Scientific Computing*; Cambridge University Press: Cambridge, UK, 1986.